

Synthesis of Mesoporous TiO₂ Induced by Nano-Cellulose and Its Photocatalytic Properties

Wei Wang, Jinpeng Wang, Xiaomeng Shi, Zhe Yu, Zhe Song, Liang Dong, Guiquan Jiang, and Shiyan Han*

Nano-cellulose was prepared *via* acid hydrolysis and cell crushing using microcrystalline cellulose as the raw material. Mesoporous TiO₂ was then prepared *via* hydrothermal synthesis using butyl titanate as the titanium source and the previously prepared nano-cellulose as the template. It is confirmed by FT-IR and XRD that the commercial product P25 consisted of anatase and rutile mixed crystal structure, in which the content of anatase and rutile was 80.5% and 19.5%, respectively. The prepared TiO₂ had an anatase single crystal structure. XPS analysis showed an elemental content of C, O, and Ti with two kinds of TiO₂. TEM, HRTEM, and electron diffraction were used to characterize the particle size of the prepared mesoporous TiO₂, mainly concentrated in the 10 to 20 nm range. Crystalline spacing was 0.35 nm (101). By comparison, the particle size of P25 was mainly distributed in the 15 to 25 nm range with a crystalline spacing of 0.35 (101) and 0.32 nm (110) respectively. XRD analysis was consistent with the results. Based on N₂ adsorption-desorption isotherm curves it was evident that the surface area of prepared TiO₂ and P25 was 38.92 m²/g and 53.54 m²/g, the cumulative pore volume of the two is 0.24 m³/g and 0.17 m³/g respectively. The experiments of photocatalytic degradation of rhodamine B showed that the catalytic ability of the prepared mesoporous TiO₂ to degrade pollutants was better than commercial TiO₂ under UV irradiation.

Keywords: Nano-cellulose; Mesoporous TiO₂; Photocatalytic degradation

Contact information: Northeast Forestry University, Material Science and Engineering Institute, Harbin 150040, Heilongjiang, China; *Corresponding author: hanshiyan80@163.com

INTRODUCTION

Nano-TiO₂ is an important semiconductor photocatalyst with many advantageous properties, including high activity for the photocatalytic degradation of organic compounds, chemical stability, as well as chemical and photochemical resistance (Wu *et al.* 2014), and non-toxic nature. This material is therefore valuable in sewage treatment and air purification applications. In recent years, mesoporous materials with pore sizes between 2 and 50 nm have been widely applied across many fields. These materials are highly suited for applications such as catalysis, separation, and adsorption because of their high specific surface area and developed pore structure. Such mesoporous materials have attracted significant research attention in the materials science field and related fields. Mesoporous molecular sieves with a hexagonal TiO₂ structure were first synthesized successfully in 1995 (Antonelli and Ying 1995); this achievement drew the attention of the research community toward mesoporous TiO₂ materials. Novel mesoporous TiO₂ materials exhibit higher catalytic activity than nano-TiO₂ (Dai *et al.* 1998; Yu *et al.* 2002; Wen 2011).

Research into mesoporous TiO₂ has made great progress. Synthetic methods have

been successfully developed for the preparation of mesoporous TiO₂ with various crystal types, pore sizes, and channel structures (orderly or disorderly), as well as good thermal stability (Li *et al.* 2014). Anatase is the major crystalline phase of TiO₂ and is commonly used in photocatalytic reactions (Augustynski 1993; Carp *et al.* 2004). Moreover, both the surface and bulk regions of TiO₂ calcined at 500 °C exist in the pure anatase form (Zhang *et al.* 2008).

Mesoporous materials are typically synthesized using organic matter as a template. The synthesis occurs *via* interfacial assembly between the inorganic species and the template agent, and the resulting materials display the narrow channel structure and narrow pore size distribution of inorganic porous materials. The surfactant template method is based on the use of molecular surfactant aggregates (capsules, *e.g.*, micelles) as templates to synthesize the desired material. The synthesis of mesoporous materials is a multidisciplinary science and is a complex process. At present, the synthesis of mesoporous TiO₂ materials is achieved using techniques including sol-gel (Antonelli and Ying 1995; Yang *et al.* 1998; Gao *et al.* 2007), microemulsion, and hydrothermal synthesis methods (Danumah *et al.* 2001; Wang *et al.* 2005; Wang *et al.* 2007). Using surfactants as a template agent, self-assembly between organic and inorganic species can be generated (Preethi *et al.* 2014).

Nano-cellulose, given its large length-to-diameter ratio, large specific area, and good biodegradability, is among the most widely used ideal template materials. The diameter of nano-cellulose ranges from 1 to 100 nm and its length is typically tens to hundreds of nanometers. Nano-cellulose can be made from natural cellulose or microcrystalline cellulose; the process involves hydrolyzing the non-crystalline regions of cellulose using concentrated sulfuric acid, liberating the cellulose nano-crystals. The nano-cellulose template synthesis method has been widely applied to produce functional materials with desirable optical, magnetic, mechanical, thermal, and/or acoustic properties (Nada and Hassan 2000; Lu *et al.* 2006; Marques *et al.* 2006; Cai *et al.* 2009; Sun *et al.* 2010).

In this study, nano-cellulose was uniformly dispersed with a networked nano-structure in aqueous solution. Because of its steric effects, the nano-cellulose plays a large role in facilitating good dispersion properties. TiO₂ typically agglomerates easily, but by using nano-cellulose, this phenomenon was avoided. The method described in this study was used to produce a novel mesoporous TiO₂ material. First, nano-cellulose was prepared using microcrystalline cellulose as a raw material. Mesoporous TiO₂ was then prepared *via* hydrothermal synthesis using tetrabutyl titanate as a titanium source.

EXPERIMENTAL

Materials

Microcrystalline cellulose, sulfuric acid, carbamide, tetrabutyl titanate (TNB), Rhodamine B (RhB), anhydrous ethanol, and commercially available TiO₂ P25 were all of analytical grade (Aladdin, China); distilled water was also used.

Preparation of Nano-Cellulose

First, 4.0 g of microcrystalline cellulose was added to a reactor, which was maintained at a constant temperature of 50 °C. Then, 200 mL of a 50% solution of sulfuric acid was added to the reactor, and the reactor was placed on a magnetic stirrer.

The reaction was carried out for 3.5 h under constant stirring. The product was washed using centrifugation until the pH of the supernatant reached approximately 6 to 7. The sediment was then removed and subjected to 15 min of splintering by a Sonifier® Cell Disrupter (Scientz JY99-IIID, Ningbo Scientz Biotechnology co., LTD, China). A nano-cellulose hydrosol was obtained from this process. The nano-cellulose hydrosol obtained was replaced with a dialysis solvent of anhydrous ethanol. This replacement process was continued until anhydrous copper sulfate (which was used to test the sample) did not exhibit a change in color.

Preparation of Mesoporous TiO₂

First, 10 mL of the aqueous suspension of nano-cellulose only containing rod-shaped cellulose species prepared in the last step described above was dissolved in 70 mL of ethanol. The resulting solution was placed in a 100-mL beaker and subjected to ultrasonication for 15 min. Then, 5 mL of butyl titanate was added. The sample was stirred uniformly and placed in a 100-mL hydrothermal synthesis reactor, which was placed in an oven and maintained at a temperature of 120 °C for 10 h. The sample was cooled, centrifuged, and washed three times each with distilled water and ethanol. After centrifugation, the treated sample was placed in the oven at 50 °C for 10 h and then calcined for 3 h in a muffle furnace at 500 °C. Mesoporous TiO₂ with good dispersibility was thus obtained.

Characterization

The structure of the mesoporous TiO₂ was confirmed using a Fourier transform infrared spectrometer (FT-IR Magna-560, Thermo Nicolet Corporation, USA). The crystal phase of the mesoporous TiO₂ was assessed by X-ray diffraction (XRD, Rigaku D/MAX 2200 VB/PC, Rigaku Corporation, Japan).

The morphologies of the nano-cellulose and the mesoporous TiO₂ particles were analyzed using transmission electron microscopy (Hitachi H-7650, Hitachi, Japan) and high-resolution TEM (HRTEM, FEI T20, FEI, USA). X-ray photoelectron spectroscopy (XPS, Thermofisher Scientific Company, K-Alpha) was used to determine the elemental composition of TiO₂,

The specific surface area of the mesoporous TiO₂ was measured using a gas adsorption instrument (Coulter Omnisorp 100CX, Beckman Coulter, USA). Nitrogen adsorption was measured at low temperature (-195.8 °C); the sample was first degassed at 300 °C for 5 h before analysis. The Brunauer-Emmett-Teller (BET) equation was used to calculate the specific surface area of the sample.

The change in the RhB's absorbance after photocatalytic degradation of the titanium dioxide was analyzed using a UV spectrophotometer (TU-1800, Purkinje General, China).

Photocatalytic Activity

The rate of degradation of Rhodamine B was measured to evaluate the photocatalytic activity of the TiO₂. First, 150 mL of a 10-mg/L Rhodamine B solution was prepared, and its UV absorption was measured at a wavelength of 550 nm. Both the solution and 50 mg of the mesoporous TiO₂ were maintained at room temperature after being added to the photocatalytic device. The pre-adsorption experiments were then carried out for 30 min under magnetic stirring and blowing air under dark conditions. Then, 10 mL of the sample was removed and centrifuged to obtain the supernatant. The

UV absorption of the supernatant was measured at 550 nm. The solution was then stirred and blown with air under ultraviolet light ($\lambda = 365$ nm, power = 8 W). Ten milliliters of the sample was removed every 30 min, and the UV absorption was measured as described above. The rate of photocatalytic degradation was calculated following the method described by Wang *et al.* (2008). Commercial TiO₂ P25 was evaluated using the same method as that used to measure the blank.

RESULTS AND DISCUSSION

TEM Analysis of Nano-Cellulose

The nano-cellulose was investigated using TEM. Examples of the resulting images are shown in Fig. 1. The TEM images showed that the nano-cellulose had a diameter of less than 20 nm with fibrous nanowires and a uniform distribution. The nano-cellulose was dispersed in solution with a networked nano-structure. Nano-cellulose is regarded as one of the most useful cellulosic biomaterials and has broad applications in the chemical industry.

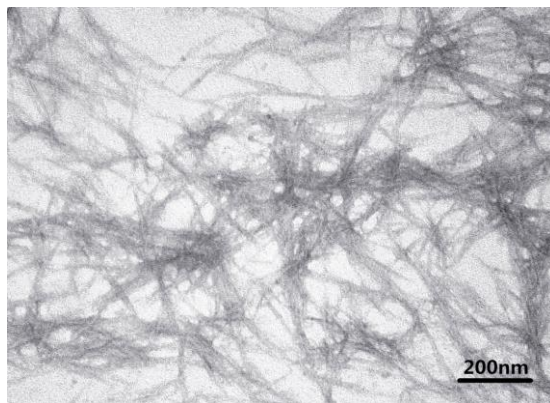


Fig. 1. TEM images of the nano-cellulose

FTIR Spectroscopy Analysis of Mesoporous TiO₂

The FTIR spectrum for the mesoporous TiO₂ is shown in Fig. 2(a). In the FTIR spectrum, the peak at 3450 cm⁻¹ was assigned to -OH stretching vibrations. The peak at around 750 to 500 cm⁻¹ was assigned to the characteristic absorption of the Ti-O bond, confirming the successful preparation of mesoporous TiO₂.

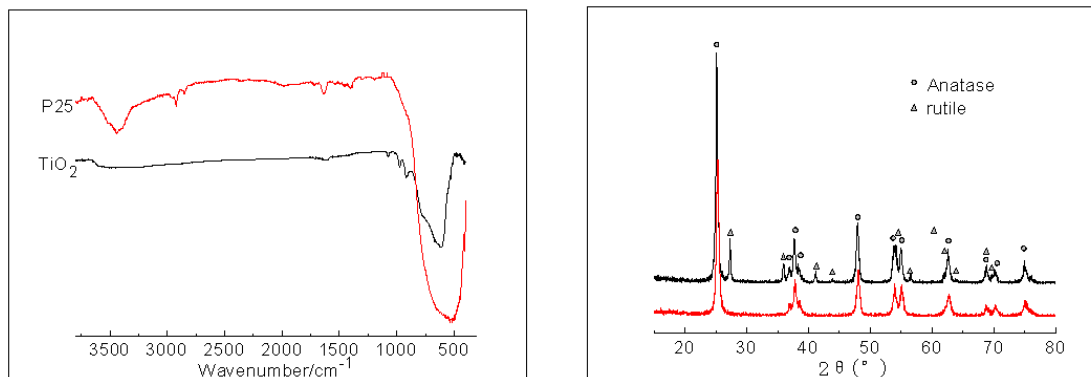


Fig. 2. (a) FTIR spectra for the TiO₂; (b) XRD patterns for the TiO₂

According to Chen and Gu (2002), the catalytic activity of nano-TiO₂ is closely related to the surface adsorption of the nanoparticles and their surface state (for example, the presence of hydroxyl groups or oxygen vacancies). Surface oxygen vacancies and the amount of surface hydroxyl groups have certain matches, so the number of hydroxyl groups directly affects the photocatalytic activity of TiO₂.

XRD Analysis of Mesoporous TiO₂

XRD patterns of the TiO₂ are shown in Fig. 2 (b). It can be seen that the diffraction peaks of the prepared TiO₂ at $2\theta=25.4^\circ$ (101), 37.86° (004), 48.82° (200), 54.14° (105), 55.38° (211), and 62.78° (204) all corresponded to anatase TiO₂, and there were no other impurity peaks. Thus, the prepared TiO₂ had a pure anatase crystalline structure. The XRD spectra of P25 showed not only the presence of diffraction peak of anatase TiO₂, but also the presence of diffraction peaks at $2\theta=27.32^\circ$ (110), 35.89° (101), 41.15° (111), 43.91° (210), 54.16° (211), and 62.4° (002), all corresponding to rutile TiO₂. HRTEM analysis showed a crystal spacing of 0.35 nm and 0.32 nm, according to the formula $X_A(\%) = 100/(1+1.265I_R/I_A)$, which makes it possible to calculate the mass fraction of anatase TiO₂ as 80.5% and the mass fraction of rutile TiO₂ as 19.5%, wherein, I_R and I_A respectively represent the intensity of diffraction peak of rutile TiO₂ (110) and anatase TiO₂ (101).

TEM Analysis of Mesoporous TiO₂

TEM and HRTEM were used to characterize the microstructure of the prepared TiO₂ and P25, as seen in Fig. 3, wherein, a, b, and c show the images of the prepared TiO₂, and d, e, and f show the images of P25. From a and d it can be seen that the two kinds of TiO₂ both consisted of spherical particles with good dispersion. The particle size of prepared TiO₂ and P25 were mainly distributed in the ranges of 10 to 20 nm and 15 to 25 nm, respectively, indicating that the nano-cellulose played a good role in the dispersion process of preparation of the TiO₂. Based on the b, c combined XRD patterns, it could be concluded that the prepared TiO₂ corresponded to an anatase crystalline structure, and the lattice spacing was 0.35 nm (101). The combined XRD patterns for e and f made it possible to conclude that the P25 had a mixed crystalline structure which was composed of anatase and rutile, and the lattice spacing was 0.35 nm (101) and 0.32 nm (110).

A synthetic simulation process is presented in Fig. 3(g). The actual synthesis results show nano-cellulose had a positive effect on the dispersion of TiO₂ and was able to prevent the agglomeration of TiO₂ particles. Cellulose is also a hydrophilic substrate, so it can promote the nucleation and growth of TiO₂ particles.

XPS Analysis of Mesoporous TiO₂

X-ray photoelectron spectroscopy (XPS) not only can determine the chemical composition of the surface, but also it can give information on the chemical state of the elements. The XPS spectra of prepared TiO₂ and P25 are shown in Fig. 4. Based on the data from XPS analysis it can be seen that the TiO₂ and P25 surfaces were composed of Ti, C, O, and other elements. A high-energy segment appeared the Auger spectrum, and the low-energy segment revealed Ti2s, O1s, Ti2p, C1s, Ti3s, Ti3p, and O2s spectral lines, which correspond to the binding energy in descending order. The peak of $E_b=458\text{eV}$, $E_b=529\text{eV}$, and $E_b=284\text{eV}$ respectively correspond to the Ti2p, O1s, and C1s, and the peak of all of the electronic energy spectra can be clearly observed.

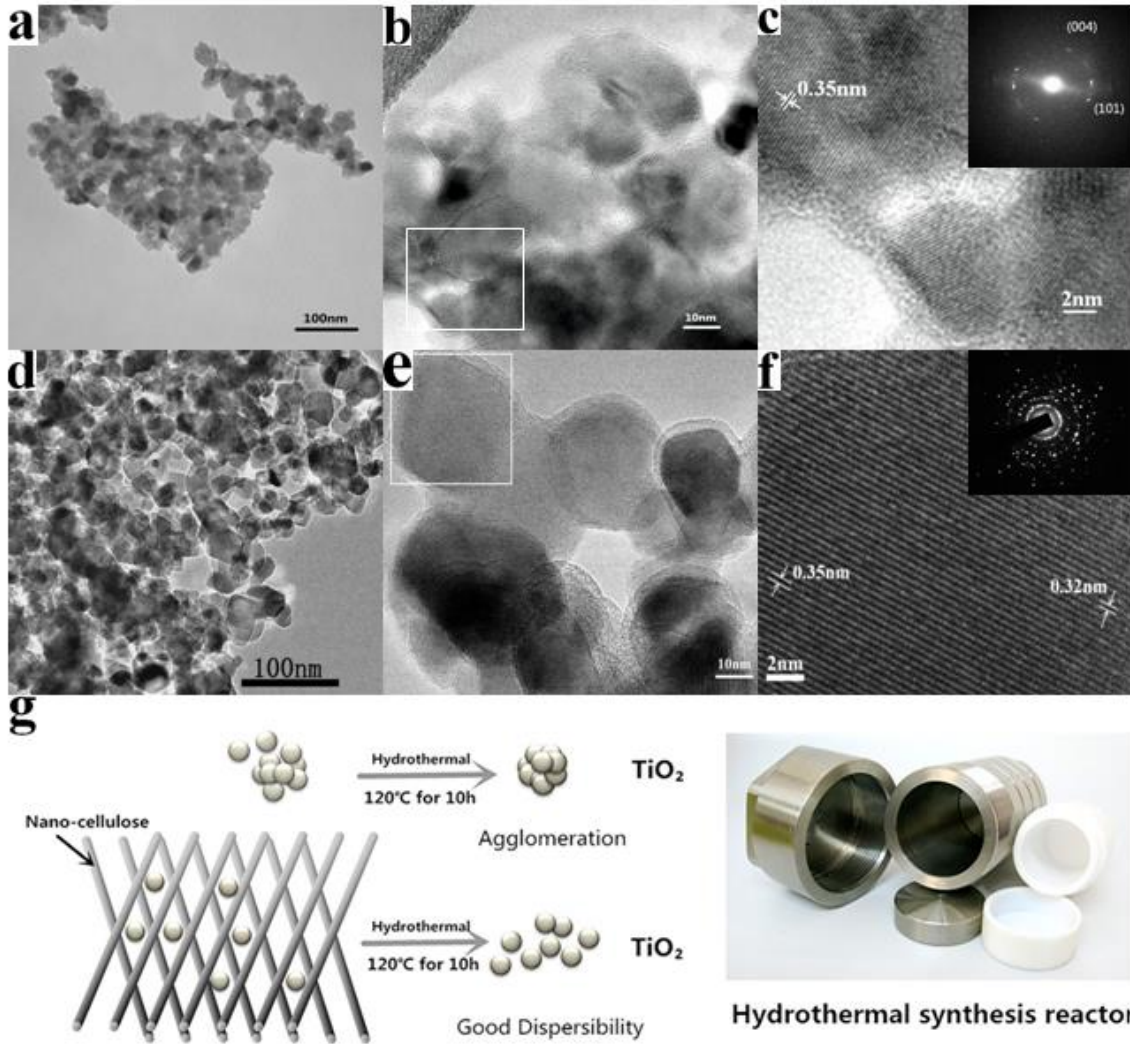


Fig. 3. TEM and HRTEM image of the TiO₂, analysis of mesoporous TiO₂ induced by nano-cellulose and the hydrothermal synthesis reactor.

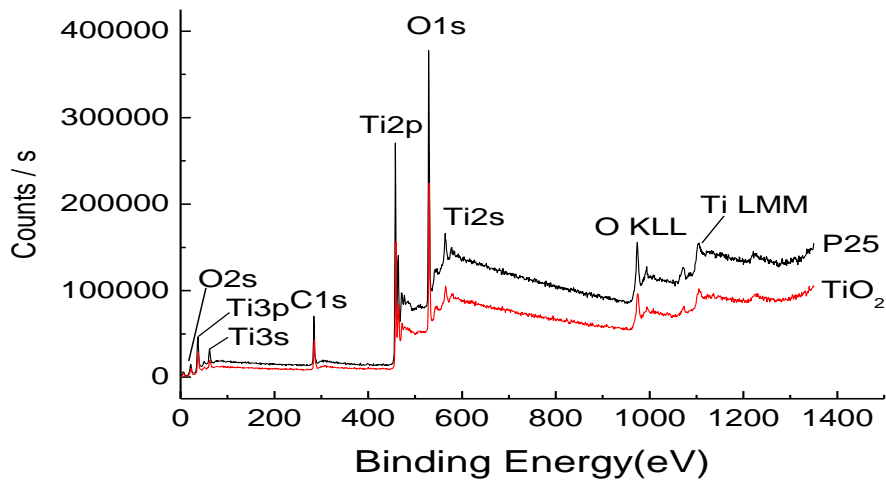


Fig. 4. XPS of TiO₂

The elements of Ti and O are mainly derived from TiO_2 , and O element also may be derived from the air, while the C element may be caused by the adsorption of CO_2 from the air. According to the elemental content analysis, the contents of C, O, and Ti of the prepared TiO_2 were 25.28%, 52.45%, and 22.27%, respectively, and the contents of C, O, and Ti of P25 were 24.53%, 52.73%, and 22.75%, respectively. From these results it can be seen that the contents of the TiO_2 and P25 were equal to each other. By the analysis of the O1s region of TiO_2 , it can be decomposed into several parts, and the main contribution comes from the Ti-O of TiO_2 , and the rest of the contribution can be attributed to the hydroxyl group as well as the adsorbed water.

Adsorption-Desorption Curve for the TiO_2

N_2 adsorption-desorption isotherm curves of the prepared TiO_2 and P25 are shown in Fig. 5. There was a non-reversible H4 type hysteresis loop in the 0.7 to 1.0 P/P_0 region. According to IUPAC classification, two H4 type hysteresis loops belong to type IV adsorption-desorption isotherms (Xu 2004). It follows that most of the pores were in the size of the mesoporous materials. Because of the mesoporous structure and the developed void space structure, the multi-layer adsorption and capillary condensation on the desorption appeared within a relative pressure range of 0.8 to 0.95, so that N_2 adsorption-desorption curve will produce hysteresis loop. Therefore, the shape of the hysteresis loop reflects the structure of a hole. Based on the N_2 adsorption-desorption isotherm curves of prepared TiO_2 , it can be found that the adsorption capacity of the prepared TiO_2 was higher than that of the P25. This may be due to the channels within the mesoporous TiO_2 particles.

Both the channels and the exposed surfaces in the gaps between particles contributed to a good adsorption performance. BET analysis showed that the surface area and pore volume of prepared TiO_2 were $38.92 \text{ m}^2/\text{g}$ and $0.24 \text{ cm}^3/\text{g}$, respectively, and the surface area and pore volume of P25 were $53.54 \text{ m}^2/\text{g}$ and $0.17 \text{ cm}^3/\text{g}$, respectively. The particle size of P25 nanoparticles perhaps was more uniform and smaller than that of TiO_2 nanoparticles, so the surface area of the former was slightly larger than that of the latter. According to the hole volume analysis, the mesoporous pores of the prepared TiO_2 may be more uniform and advanced than those of P25, so the accumulated pore volume of the prepared TiO_2 was relatively large, which may be more favorable for the adsorption.

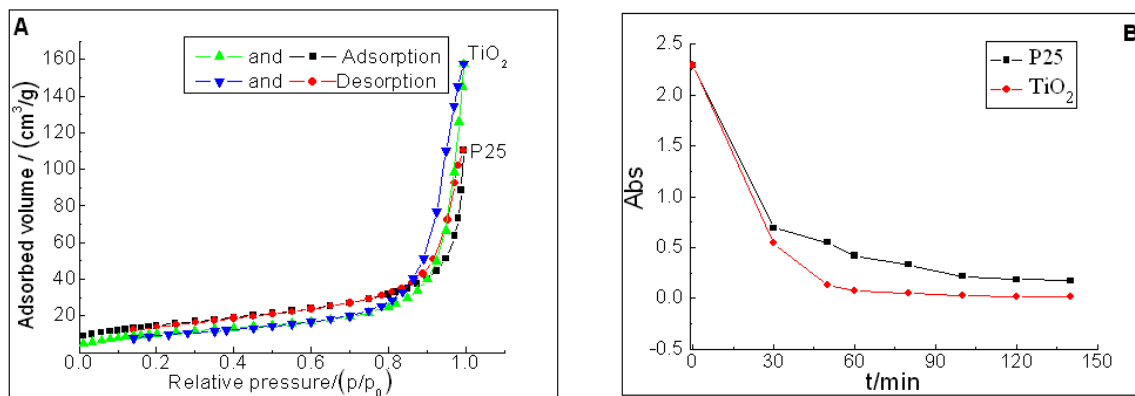


Fig. 5. (a) Nitrogen adsorption-desorption isotherm of mesoporous TiO_2 ; (b) The photocatalytic degradation curve for the mesoporous TiO_2

Photocatalytic Analysis of Mesoporous TiO₂

The organic dye rhodamine B was used as a simulation of pollutants. As shown in Fig. 5, there was evident degradation of rhodamine B under ultraviolet light (wavelength = 365 nm, power = 8 W). Experimental results showed that in the pre-adsorption of 0.5 h, the prepared TiO₂ was better than P25, which provides further evidence that the porosity of the prepared TiO₂ was more advanced than that of P25. When it is accompanied by blowing, stirring, and UV irradiation, with the time extension, the prepared TiO₂ and P25 exhibited different degrees of catalytic degradation. The degradation rate of TiO₂ and P25, respectively, were 96.9 % and 77.3 % after degradation for 1 h. After 2 h, the degradation rate was 98.9% and 90.7%, respectively. These results further indicate that the degradation of the pollutants in the prepared TiO₂ was greater than that of P25. According to research findings, pure rutile TiO₂ structure provides stability, but the catalytic activity is lower than that of pure anatase TiO₂ (Shi and Weng 2008; Kandiel *et al.* 2010); For a mixed crystalline structure of TiO₂, the mixed crystal effect is not a simple anatase and rutile mixture; rather the surface consisted of a thin rutile layer. An internal anatase phase was coated with mixed crystal structure, and the contents of rutile directly influenced the anatase excited valence electron optical line. According to a report, the optimal photocatalytic activity of the mixed crystal TiO₂ is the best when the content of anatase reaches 60% (Shi and Weng 2008). The content of anatase in P25 was 80.5%, which much higher than the share of the optimal ratio of anatase. However, because of the presence of rutile TiO₂, the photocatalytic degradation ability was decreased, leading to the catalytic activity of the prepared pure anatase TiO₂ being better than the P25 mixed crystal structure.

CONCLUSIONS

1. Nano-cellulose with a particle size of less than 20 nm was prepared using acid hydrolysis and splintering by Sonifier® Cell Disrupter. Microcrystalline cellulose was used as a raw material. Mesoporous TiO₂ was prepared *via* hydrothermal synthesis using butyl titanate as a titanium source, and the as-prepared nano-cellulose was used as a template.
2. It was confirmed that the commercial P25 consisted of anatase and rutile mixed crystal structure by FT-IR and XRD, in which the content of anatase and rutile was 80.5% and 19.5% respectively; the prepared TiO₂ had an anatase single crystal structure. XPS analysis showed the elemental content of C, O, and Ti, with two kinds of TiO₂.
3. TEM was used to characterize the microstructure of the prepared TiO₂ and P25. The results showed that both kinds of TiO₂ consisted of spherical particles with good dispersion. The particle size of the prepared TiO₂ and P25 were mainly distributed in the size ranges of 10 to 20 nm and 15 to 25 nm, respectively. Both species of TiO₂ particles were dispersed as singlet particles with no evidence of reunion phenomena. HRTEM further confirmed that the prepared TiO₂ corresponded with the anatase crystalline structure, and the lattice spacing was 0.35 nm (101), and the P25 had a mixed crystalline structure incorporating both anatase and rutile, and the lattice spacing was 0.35 nm (101) and 0.32 nm (110).

4. BET analysis showed that the surface area and pore volume of prepared TiO₂ were 38.92 m²/g and 0.24 cm³/g, respectively, and the surface area and pore volume of P25 were 53.54 m²/g and 0.17 cm³/g, respectively.
5. Photocatalytic degradation of rhodamine B results showed that when the UV photocatalytic degradation was carried out for 1 h, the prepared TiO₂ was degraded completely to some extent, its catalytic ability to degrade pollutants was better than the commercial P25.

ACKNOWLEDGMENTS

This work was supported by the Fundamental Research Funds for the Central Universities (2572014CB03), the Young Technology Innovation Talent Foundation of Harbin (2013RFQXJ035), Young Science Foundation of Heilongjiang (QC2013C033), and the Key Projects of Science and Technology Department of Jilin Province (20140204006GX).

REFERENCES CITED

- Antonelli, D. M., and Ying, J. Y. (1995). "Synthesis of hexagonally packed mesoporous TiO₂ by a modified sol-gel methods," *Angew. Chem. Int. Ed. Eng.* 34(18), 2014-2017. DOI: 10.1002/anie.199520141
- Augustynski, J. (1993). "The role of the surface intermediates in the photoelectron-chemical behaviour of anatase and rutile TiO₂," *Electrochim. Acta.* 38(1), 43-46. DOI: 10.1016/0013-4686(93)80008-N
- Cai, J., Kimura, S., and Wada, M. (2009). "Nanoporous cellulose as metal nanoparticles Support," *Biomacromolecules* 10(1), 87-94. DOI: 10.1021/bm800919e
- Carp, O., Huisman, C. L., and Reller, A. (2004). "Photoinduced reactivity of titanium dioxide," *Prog. Solid State Chem.* 32(1-2), 33-177. DOI: 10.1016/j.progsolidstchem.2004.08.001
- Chen, X. Q., and Gu, G. B. (2002). "Preparation of nanometer crystal TiO₂ of high photocatalytic activity with titanil organic compound as precursor," *Chin. J. Catal.* 23(4), 312-316. DOI: 10.3321/j.issn:0253-9837.2002.04.007
- Dai, Q., He, N. Y., and Guo, Y. (1998). "High photocatalytic activity of pure TiO₂ mesoporous molecular sieves for the degradation of 2, 4, 6-trichlorophenol," *Chem. Lett.* 11(1), 1113. DOI:10.1246/cl.1998.1113
- Danumah, C., Vaudrouil, S., and Bonneviot, L. (2001). "Synthesis of macrostructured MCM-48 molecular sieves," *Micropor. Mesopor. Mater.* 44(1), 241-247. DOI: 10.1016/S1387-1811(00)00287-0
- Kandiel, T.A., Feldhoff, A., Robben, L., Dillert, R., and Bahnemann, D. W. (2010). "Tailored titanium dioxide nanomaterials: Anatase nanoparticles and brookite nanorods as highly active photocatalysts," *Chem. Mater.* 22(6), 2050-2060. DOI:10.1021/cm903472p.
- Li, W., Wu, Z. X., and Wang, J. X. (2014). "A perspective on mesoporous TiO₂ materials," *Chem. Mater.* 26(1), 287-289. DOI: 10.1021/cm4014859
- Lu, Q. Y., Gao, F., and Komarneni, S. (2006). "Cellulose-directed growth of selenium

- nanobelts in solution,” *Chem. Mater.* 18(1), 159-163. DOI: 10.1021/cm051082z
- Marques, P. A. A. P., Trindade, T., and Neto, C. P. (2006). “Titanium dioxide/cellulose nanocomposites prepared by a controlled hydrolysis method,” *Compos. Sci. Technol.* 66(7-8), 1038-1044. DOI: 10.1016/j.compscitech.2005.07.029
- Nada, A. M. A., and Hassan, M. L. (2000). “Thermal behavior of cellulose and some cellulose derivatives,” *Polym. Degrad. Stab.* 67(1), 111-115. DOI: 10.1016/S0141-3910(99)00100-7
- Preethi, T., Abarna, B., and Rajarajeswari, G. R. (2014). “Influence of chitosan–PEG binary template on the crystallite characteristics of sol–gel synthesized mesoporous nano-titania photocatalyst,” *Appl. Surf. Sci.* 317, 90-97. DOI:10.1016/j.apsusc.2014.07.190
- Shi, L., and Weng, D. (2008). “Highly active mixed-phase TiO₂ photocatalysts fabricated at low temperature and the correlation between phase composition and photocatalytic activity,” *J. Environ. Sci.* 20(10), 1263-1267. DOI:10.3321/j.issn:1001-742.2008.10.017
- Sun, D. P., Yang, J. Z., and Wang, X. (2010). “Bacterial cellulose/TiO₂ hybrid nanofibers prepared by the surface hydrolysis method with molecular precision,” *Nanoscale* 2(2), 287-292. DOI: 10.1039/b9nr00158a. Epub 2009 Nov 11
- Wang, R. W., Xu, L., and Zhao, L. (2005). “Synthesis, characterization and catalytic activities of mesostructured aluminophosphates assembled with preformed MFI zeolite nanoclusters,” *Micropor. Mesopor. Mater.* 83(1), 136-139.
- Wang, J., Fan, M. Q., Liu, Y. F., Jing, X. Y., Zhang, M. I., and Liu, T. F. (2007). “Novel functional material: Synthesis and characterization of magnetic solid superacid SO₄²⁻/ZrO₂-MgO-Fe₃O₄,” *J. Funct. Mater.* 38(1), 78-80.
- Wang, X. J., Liu, C. Z. H., and Hu, Z. H. (2008). “Preparation, characterization and photocatalytic performance of porous TiO₂ micro-beads,” *J. Catal.* 29(4), 391-396.
- Wu, T. S., Sun, H. Y., Hou, X., Liu, L. H., Zhang, H. M., and Zhang, J. J. (2014). “Significant room-temperature ferromagnetism in porous TiO₂ thin films,” *Micropor. Mesopor. Mater.* 190(15),:63-66. DOI:10.1016/j.micromeso.2014.01.024
- Xu, R. R. (2004). *Molecular Sieve and Porous Material Chemistry*, Science Press, Beijing, China.
- Yang, P. D., Zhao, D. Y., and Matgolese, D. I. (1998). “Generalized syntheses of large-pore mesoporous metal oxides with semicrystalline frameworks,” *Nature* 396(1), 152-155. DOI: 10.1038/24132
- Yu, J. C., Zhang, L. Z., and Yu, J. G. (2002). “Rapid synthesis of mesoporous TiO₂ with high photocatalytic activity by ultrasound-induced agglomeration,” *New J. Chem.* 120(4), 416-420. DOI: 10.1039/b109173e
- Zhang, J., Xu, Q., and Feng, Z. C. (2008). “Importance of the relationship between surface phases and photocatalytic activity of TiO₂,” *Angew. Chem. Int. Ed.* 47(9), 1790-1793. DOI: 10.1002/ange.200704788

Article submitted: May 7, 2015; Peer review completed: August 24, 2015; Revised version received: January 16, 2016; Accepted: January 20, 2016; Published: February 8, 2016. DOI: 10.15376/biores.11.2.3084-3093